

Multi-channel architecture for electronic quantum-Hall interferometry

Vittorio Giovannetti¹, Fabio Taddei¹, Diego Frustaglia², and Rosario Fazio^{3,1}

¹*NEST-CNR-INFM and Scuola Normale Superiore, I-56126 Pisa, Italy*

²*Departamento de Física Aplicada II, Universidad de Sevilla, E-41012 Sevilla, Spain*

³*International School for Advanced Studies (SISSA), I-34014 Trieste, Italy*

(Dated: October 27, 2018)

We propose a new architecture for implementing electronic interferometry in quantum Hall bars. It exploits scattering among parallel edge channels. In contrast to previous developments, this one employs a simply-connected mesa admitting serial concatenation of building elements closer to optical analogues. Implementations of Mach-Zehnder and Hanbury-Brown-Twiss interferometers are discussed together with new structures yet unexplored in quantum electronics.

PACS numbers: 72.25.-b, 85.75.-d, 74.50.+r, 05.70.Ln

Since many decades interferometry has been a fundamental tool to disclose the classical and quantum properties of light [1]. Nowadays optical interferometry can be considered at the heart of a new quantum-based technology with applications in metrology [2], imaging [3], and quantum information processing [4]. In the solid state world, controlled quantum interference experiments appeared more recently when, thanks to the advances in fabrication, the wave-like nature of electrons could be tested in transport measurements. The observation of Aharonov-Bohm (AB) oscillations in the electric current [5] and the Landauer-Büttiker formulation of quantum transport in terms of electronic transmission amplitudes [6] signaled the beginning of quantum electronic interferometry in solid state devices. Since then, there has been a continuous effort in studying interference effect in quantum transport [7]. A recent breakthrough in electronic interferometry has been the experimental realization of electronic Mach-Zehnder [8, 9, 10, 11, 12] (MZ) and Hanbury-Brown-Twiss (HBT) [13] interferometers using edge states in a quantum Hall bar. In these experiments electrons loop around an annular (Corbino-like) sample flowing along chiral edge channels which mimic the optical paths [14]. In order to unfold the full potentiality of optical interferometry in the solid state realm an important additional ingredient is needed: The ability to concatenate in series several MZ interferometers. This requirement, impossible to implement at present, leads us to develop a new interferometric architecture for edge states. This scheme opens up a wide range of new possibilities in electronic interferometry. As first examples we discuss implementations of the MZ, HBT, and *interaction-free* [15] interferometers. Furthermore we show how to exploit our setup for characterizing the sources of dephasing in quantum Hall systems.

A good starting point to present our new architecture is to consider the MZ configuration. In an optical MZ interferometer (inset Fig. 1), a monochromatic beam from source 1a is split into two beams by a beam splitter BS₁. The beams then propagate along two different paths which recombine at a second beam splitter BS₂, where interference occurs. The two outgoing beams are collected at detectors 2a and 2b. In the absence of external noise, the beam intensity at the detectors exhibits oscillations as a function of the accumulated phase difference between the followed paths. Our electronic implementation of the MZ interferometer is sketched in Fig. 1. It consists of a 2DEG subject to a quantizing perpendicular magnetic field B corresponding to a filling factor (number of occupied Landau levels) $\nu \equiv n_s h / eB = 2$. Four electronic contacts are present in the structure: A bias voltage V is applied to 1a, acting as a source, while the remaining contacts 1b, 2a and 2b are grounded. The shadowed regions in the figure rep-

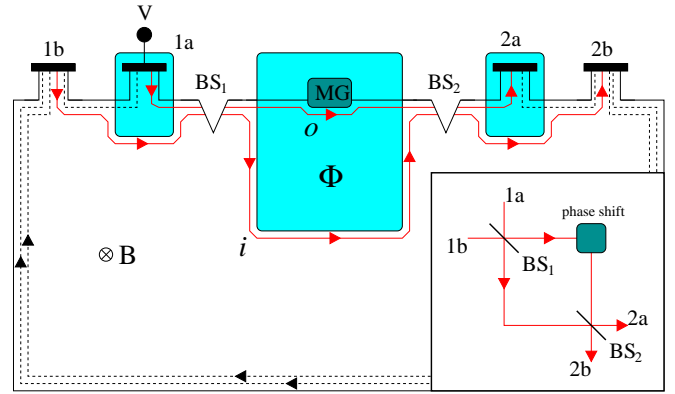


FIG. 1: (color online) Mach-Zehnder interferometer implementation. The shaded areas represent top gates which define regions of filling factor $\nu = 1$. In the rest of the sample instead we assume $\nu = 2$. Due to the presence of a strong magnetic field B orthogonal to the bar surface, electrons injected from the source contact 1a propagate from left to right following two possible paths. Electrons are finally collected at drain contacts 2a and 2b, where currents are measured. The red lines represent the edge channels effectively taking part to the MZ interferometer. BS₁ and BS₂ are beam splitters, while the gate MG is used to vary the shape and length of the outer edge o channel. Notice that an experimental implementation of the setup does not require to employ air-bridge elements. Inset: sketch of the optical counterpart of the MZ interferometer.

ter BS₂, where interference occurs. The two outgoing beams are collected at detectors 2a and 2b. In the absence of external noise, the beam intensity at the detectors exhibits oscillations as a function of the accumulated phase difference between the followed paths. Our electronic implementation of the MZ interferometer is sketched in Fig. 1. It consists of a 2DEG subject to a quantizing perpendicular magnetic field B corresponding to a filling factor (number of occupied Landau levels) $\nu \equiv n_s h / eB = 2$. Four electronic contacts are present in the structure: A bias voltage V is applied to 1a, acting as a source, while the remaining contacts 1b, 2a and 2b are grounded. The shadowed regions in the figure rep-

resent top gates which reduce the local electron density n_s in such a way that the filling factor in the underneath regions is $\nu = 1$. Such cross-gate technique, implemented e.g. in Refs. [16, 17, 18], is used to selectively address the two edge channels by introducing a spatial separation between them. In particular, the gate on top of 1a allows us to selectively populate only the outer edge o of the sample by preventing the inner channel i to be subject to the bias voltage V . Analogously, the gate on top of the contact 2a allows us to measure the current carried by the outer edge channel only. Finally the large top gate in the center of the setup induces a spatial separation between the two edge states. The area A defined by the two paths encloses a magnetic flux $\Phi = BA$. It is important to notice that such an area can be substantially smaller as compared with other MZ realizations [8, 9, 10, 11, 12, 13]. In our proposed architecture values of $A \sim 1 \mu\text{m}^2$ (corresponding to about 10^3 flux quanta) are experimentally feasible with present technology. This is an improvement of almost two orders of magnitude with respect to conventional MZ setups that would arguably lead to a reduced effect of phase averaging due to area and/or flux fluctuations (as stated in Ref. [13], where a visibility enhancement was ascribed to a size reduction with respect to previous implementations [8]).

Beam splitter transformations among the edges o and i are introduced, as in Ref. [19], by inducing elastic inter-channel scattering within the regions BS_1 and BS_2 of Fig. 1. This is admittedly the most delicate part of our proposal. There are however two ways to implement it. Inter-channel scattering can be obtained by an abrupt (non-adiabatic) variation in the confining potential such as the triangular-shaped protuberance shown in the figure. According to the calculations of Ref. [20], edge channels mix coherently if the (potential defining) the protuberance shows spatial inhomogeneities on a scale smaller than the magnetic length $l_m = \sqrt{\hbar/eB}$. Such potential profiles can be engineered to give the desired scattering amplitude, for example, by the cleave-edge overgrowth technique [21]. Another possibility to have elastic inter-channel scattering is to use high-spatial-resolution local probes as atomic force microscopy [22] or scanning gate microscopy [23]. In this way there is the additional advantage that the scattering amplitudes can be tuned by means of an external voltage.

As in Refs. [8, 9, 10, 11, 12, 13], we assume the size of the structure to be much smaller than the equilibration length at which spontaneous inter-channel mixing occurs [17]. Moreover, apart from a small region where the BSs are implemented, the confining potential is assumed to be sufficiently smooth to prevent undesired inter-channel scattering. Under these conditions, o and i represent two independent electronic modes of propagation which play the role of optical paths in a MZ interferometer.

To have a first glimpse of the extreme versatility of

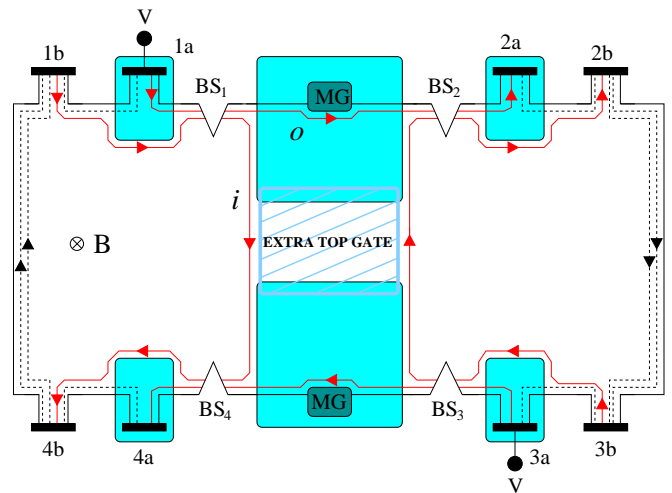


FIG. 2: (color online) Implementation of the Hanbury-Brown-Twiss interferometer.

this new architecture we notice that the setup of Fig. 1 can be turned easily into a HBT interferometer — see Fig. 2. The resulting implementation is reminiscent of the one realized by Neder *et al.* with the traditional (non simply connected) mesa configuration [13]. In our case it has been obtained by introducing a further MZ interferometer in the bottom part of the mesa of Fig. 1, allowing the central top gates to overlap (possibly with the help of the extra top gate shown in the figure).

Additionally, very interesting devices with no counterpart in conventional edge state setups can be devised by fully exploiting the concatenability of our simply connected architecture. A first example is sketched in Fig. 3. This is an electronic equivalent of the optical *interaction-free* interferometer of Ref. [15] (see the caption of Fig. 3 for a brief description of its working principles). With our architecture we can reproduce it by properly concatenating a series of MZs of Fig. 1.

A further interesting application is found in the characterization of dephasing in quantum Hall systems which is recently attracting a lot of interest [8, 9, 10, 11, 12, 24, 25, 26]. Consider first the setup of Fig. 1. The transmission probability $T_a(E)$ from terminal 1a to 2a, reads

$$T_a(E) = T_{1o}T_{2o} + R_{1o}R_{2i} + 2\sqrt{T_{1o}T_{2o}R_{1o}R_{2i}} \cos[\Delta\phi(E)], \quad (1)$$

where for $\alpha = o, i$ and $j = 1, 2$, $T_{j\alpha}$ and $R_{j\alpha} = 1 - T_{j\alpha}$ are, respectively, the transmission and the reflection probabilities of the beam splitter BS_j . A similar expression can be obtained for T_b (transmission from 1a to 2b). The last contribution in Eq. (1) is an interference term leading to current oscillations at the contact 2a. It accounts for the phase difference $\Delta\phi$ associated to the two possible paths the electrons can choose in their propagation. Apart from an irrelevant constant term, in the absence

of external noise it can be expressed as

$$\Delta\phi(E) = \phi_D(E) + \phi_{AB}. \quad (2)$$

The first term is a dynamical contribution given by [24] $\phi_D(E) = E\Delta L/\hbar v_D$, where ΔL is length difference between the paths (for simplicity we assume the channels o and i to have identical drift velocities). The second term in Eq. (2) is the AB contribution $\phi_{AB} = 2\pi e\Phi/h$. Both the dynamical and the AB contributions can be varied in our setup by modifying the shape of the outer path by means of the local gate MG of Fig. 1. Decoherence can be described by adding an extra term φ in Eq.(2) which accounts for possible phase fluctuations. These may originate either from long time oscillations of locally trapped impurities or thermal fluctuations of the edge-state local density. Decoherence eventually leads to the suppression of the interference term in $T_{a,b}(E)$, Eq. (1), thus reducing the visibility of the oscillations induced by the modulation of the gate MG in the output currents [6] $I_{a,b} \equiv (e/h) \int dE [f(E - eV) - f(E)] T_{a,b}(E)$. Notably the visibility can be suppressed even in the absence of decoherence. This is due to the energy dependence of the phase, giving rise to a phase-averaging of the current $I_{a,b}$ when integrating over a large energy window [24]. The visibility decrease has been intensively investigated in these systems [8, 9, 10, 11, 24, 25, 26] trying to identify its sources by means of shot noise measurement [8]. No information can be obtained just from the average current by using a MZ single interferometer. Our architecture makes possible to discriminate between phase-averaging and decoherence mechanisms directly in the measurement of the average current by concatenating two MZ interferometers. The setup is shown in Fig. 4. For the sake of simplicity we assume $T_{1,2\alpha} = R_{1,2\alpha} = 1/2$. The transmission between 1a and 2a for this device reads

$$T_a(E) = 1/2 + (R_{3o} - T_{3o}) \cos[\Delta\phi_1(E) + \varphi_1]/2 \quad (3) \\ + \sqrt{R_{3o}T_{3o}} \sin[\Delta\phi_1(E) + \varphi_1] \sin[\Delta\phi_2(E) + \varphi_2],$$

with $\Delta\phi_{1,2}(E)$ defined, as in Eq. (2), in terms of the parameters $\Delta L_{1,2}$ and $\Phi_{1,2}$ associated with the two large gated areas of Fig. 4. The $\varphi_{1,2}$ account for corresponding noise fluctuations. In the linear-response regime at zero temperature, contact 2a receives an output current $I_a = (e^2V/2h)[1 + (R_{3o} - T_{3o})\kappa_1 + 2\sqrt{R_{3o}T_{3o}}\kappa_2]$ with

$$\kappa_1 = \int_0^{eV} \frac{dE}{eV} \cos[\Delta\phi_1(E) + \varphi_1], \\ \kappa_2 = \int_0^{eV} \frac{dE}{eV} \sin[\Delta\phi_1(E) + \varphi_1] \sin[\Delta\phi_2(E) + \varphi_2].$$

Regarding decoherence, we treat it in a phenomenological fashion by defining a zero-temperature distribution of phase fluctuations $P(\varphi_1, \varphi_2)$, such that the average current reads $\langle I_a \rangle = \int d\varphi_1 d\varphi_2 P(\varphi_1, \varphi_2) I_a$. In the uncorrelated case [i.e. $P(\varphi_1, \varphi_2) = P_1(\varphi_1)P_2(\varphi_2)$] with Gaussian

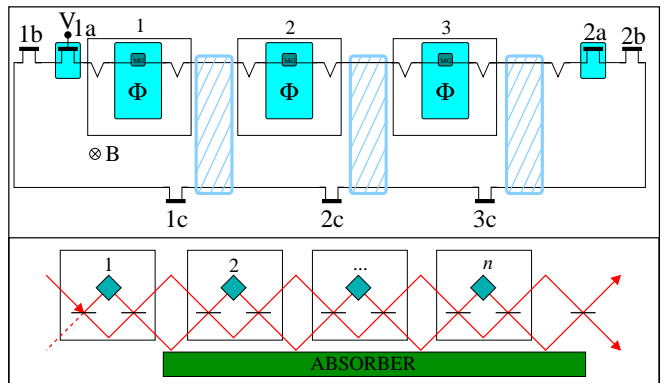


FIG. 3: (color online) *Interaction-free* interferometer. The optical implementation is shown in the lower part of the graph. It consists in a series of n concatenated MZ interferometers characterized by a phase difference $\phi = \pi/n$ among the two internal paths [15]. One of the two emerging paths from each of the MZ impinges into an external absorber (the green box in the picture) which can be either totally reflecting ($\eta = 1$) or totally absorbing ($\eta = 0$). Incoming photons deterministically end up either in the upper or the lower exit port depending on η . The electronic implementation of this device for $n = 3$ is found in the upper part of the picture. Here the “absorber” is simulated by the grounded contacts 1c, 2c and 3c. The absorption ($\eta = 0$) case is simulated by switching on extra top gates (patterned areas in the figure) which put in contact the inner edge with 1c, 2c and 3c.

phase-fluctuations (of width $\sigma_{1,2}$) we find

$$\langle I_a \rangle = \frac{e^2V}{2h} [1 + (R_{3o} - T_{3o})\tilde{\kappa}_1 D_1 + 2\sqrt{R_{3o}T_{3o}}\tilde{\kappa}_2 D_1 D_2],$$

where $D_{1,2} \equiv \exp[-\sigma_{1,2}^2/2]$, $\tilde{\kappa}_1 \equiv \kappa_1(\varphi_1 = 0)$ and $\tilde{\kappa}_2 \equiv \kappa_2(\varphi_2 = 0)$. We see that $\langle I_a \rangle$ has two interference terms proportional to $\tilde{\kappa}_1$ and $\tilde{\kappa}_2$, respectively. The interference terms vanish *only* in the presence of full decoherence ($D_{1,2} = 0$): Strong phase averaging (large voltages) reduces $\tilde{\kappa}_1$ to zero, but geometrical correlations between $\Delta\phi_1$ and $\Delta\phi_2$ can preserve $\tilde{\kappa}_2$ from that (for instance, the case $\Delta L_1 = \Delta L_2$ and $\Phi_1 = \Phi_2$ yields $\tilde{\kappa}_2 \simeq 1/2$). This is strikingly different from the results of a single MZ interferometer, where complete phase averaging leads to the suppression of any interference term in the current and hence one has to resort to shot noise measurements. For illustration, we provide an example in Fig. 5. There we plot the linear conductance $G_a \equiv \langle I_a \rangle/V$ as a function of the magnetic field for small voltages $eV \ll \hbar v_D/\Delta L_1$ (red curve) and for large voltages $eV \gg \hbar v_D/\Delta L_1$ (blue curve) in the presence of a small decoherence ($D_{1,2} \simeq 1$). Oscillations are suppressed as voltage increases due to the voltage dependence of $\tilde{\kappa}_{1,2}$. For large voltages (blue curve), the conductance converges to a constant value $G_a = \frac{e^2}{2h} [1 + D_1 D_2 \sqrt{R_{3o}T_{3o}}]$ depending only on decoherence through $D_{1,2}$. In the case of strong decoherence G_a takes the universal value $e^2/2h$ (black curve) showing no voltage dependence. A similar analysis was presented

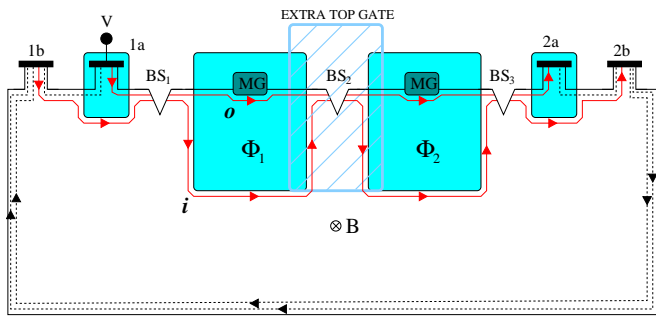


FIG. 4: (color online) Example of two MZ interferometers concatenated. The two large shaded areas are characterized respectively by AB fluxes Φ_1 and Φ_2 and path-length differences $\Delta L_{1,2}$. The patterned area represents an auxiliary top gate which can be inserted to bypass the second BS, converting the whole setup to a single MZ interferometer of Fig. 1.

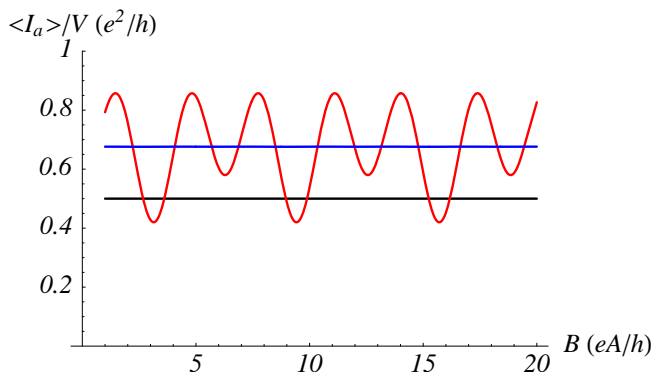


FIG. 5: (color online) Linear conductance $G_a = \langle I_a \rangle / V$ as a function of magnetic field B for different values of voltage V , with $D_1 = 0.8$, $D_2 = 0.9$, $R_{3u} = 0.4$, $T_{3u} = 0.6$, $\Delta L_1 / \Delta L_2 - 1 = 10^{-4}$. Red (blue) curve is relative to a small (large) voltage, while the black curve is the completely incoherent case (i.e. $D_{1,2} = 0$).

in Ref. [8]. In that case, shot-noise measurements were needed. It is also worth noticing that the configuration of Fig. 4 can be used to explore possible spatial correlations between the fluctuations in the two different MZ interferometers.

The architecture presented in this paper, once realized experimentally, may open up a way to an entire new class of electronic interferometry. We gave three examples, all based on the concatenation of several MZ interferometers. This proposal can be easily generalized to filling factors higher than 2, which would allow the implementation of complex multi-mode interferometry. This, along with the ability of multiple concatenation of interferometers, could yield prototypical implementation of simple linear-optics-like quantum computing [4] devices, or be

relevant in revealing non-Abelian statistics in the fractional Quantum Hall regime [27]. Moreover, by properly tuning the BS transparencies, the setup of Fig. 1 yields a edge-channel swapper. Alternatively, it can be employed to prepare controlled superpositions of the two outgoing edge channels.

We thank M. Heiblum, F. Marquardt, V. Piazza and S. Roddaro for comments and discussions. We acknowledge financial support from the EU funded NanoSciERA “NanoFridge” and RTNNANO projects, and the “Ramón y Cajal” program of the Spanish Ministry of Education and Science.

-
- [1] M. O. Scully and M. S. Zubairy, *Quantum Optics* (Cambridge Univ. Press, Cambridge, 1997).
 - [2] V. Giovannetti, S. Lloyd, L. Maccone, *Science* **306**, 1330 (2004).
 - [3] Y. Shih, Eprint arXiv:0707.0268.
 - [4] E. Knill, R. Lafamme and G. J. Milburn, *Nature* **409**, 46 (2001)
 - [5] D. Y. Sharvin and Y. V. Sharvin, *JETP Lett.* **34**, 272 (1981); R. A. Webb *et al.*, *Phys. Rev. Lett.* **54**, 2696 (1985).
 - [6] M. Büttiker *et al.*, *Phys. Rev. B* **31**, 6207 (1985); M. Büttiker, *ib.* **38**, 9375 (1988).
 - [7] S. Datta, *Electronic Transport in Mesoscopic Systems* (Cambridge Univ. Press, Cambridge, 2005).
 - [8] Y. Ji, *et al.*, *Nature* **422**, 415 (2003).
 - [9] I. Neder, *et al.*, *Phys. Rev. Lett.* **96**, 016804 (2006).
 - [10] L. V. Litvin, *et al.*, *Phys. Rev. B* **75**, 033315 (2007).
 - [11] P. Roulleau, *et al.*, arXiv:0704.0746 (preprint).
 - [12] I. Neder *et al.*, *Nature Physics* **3**, 534 (2007).
 - [13] I. Neder, *et al.*, *Nature* **448**, 333 (2007).
 - [14] B. I. Halperin, *Phys. Rev. B* **25**, 2185 (1982); M. Büttiker, *Phys. Rev. B* **38**, 9375 (1988).
 - [15] J. -S. Jang, *Phys. Rev. A* **59** 2322, (1999).
 - [16] R. J. Haug, *et al.*, *Phys. Rev. Lett.* **61**, 2797 (1988); S. Washburn, *et al.*, *ibid.* **61**, 2801 (1988).
 - [17] R. J. Haug, *Semicond. Sci. Technol.* **8**, 131 (1993).
 - [18] A. Würtz, *et al.* *Phys. Rev. B* **65**, 075303 (2002).
 - [19] C. W. J. Beenakker, *et al.* *Phys. Rev. Lett.* **91**, 147901 (2003).
 - [20] J. J. Palacios and C. Tejedor, *Phys. Rev. B* **45**, 9059 (1992); *ibid.* **48**, 5386 (1993); O. Olenksi and L. Mikhailovska, *Phys. Rev. B* **72**, 235314 (2005).
 - [21] L. Pfeiffer, *et al.* *Appl. Phys. Lett.* **56**, 1697 (1990).
 - [22] M. T. Woodside, *et al.* *Phys. Rev. B* **64**, 041310 (2001).
 - [23] N. Aoki, *et al.* *Phys. Rev. B* **72**, 155327 (2005).
 - [24] V. S. -W. Chung, P. Samuelsson, and M. Büttiker, *Phys. Rev. B* **72**, 125320 (2005).
 - [25] F. Marquardt and C. Bruder, *Phys. Rev. B* **70**, 125305 (2004).
 - [26] I. Neder and F. Marquardt, *New J. Phys.* **9**, 112 (2007).
 - [27] K.T. Law, Eprint arXiv:0707.3995.